# The Mechanism of Air Entrainment in the Slot Die Coating Process

**Sima Didari, Zakaria Y. Ahmad, James D. Veldhorst, Tequila A.L. Harris[a]**
a: corresponding author: tequila.harris@me.gatech.edu, Georgia Institute of Technology, Woodruff School of Mechanical Engineering, Atlanta, Georgia 30332, USA

## 1. Introduction

Slot die casting is one of the best methods of manufacturing thin film because of its ability to produce uniform films, from solution, with the preset thickness ranging from 5 to 200μm [1]. The final quality of the cast film depends on the operational conditions such as web speed and the flow rate of the cast solution. The range of the operational conditions resulting in the manufacturer of defect free films is called casting window [2-4] . Outside this region different types of defects such as holes, break-lines, ribbing and air entrainment have been observed and reported by numerous studies[5-12]. Among all these defects air entrainment is of paramount importance due to the limitation imposed to the maximum speed of the casting. Several researchers have extensively studied the prediction of the casting window for the slot die casting process at different operating conditions, in the past. However, few studies exist focusing on the investigation of the air engulfment phenomenon, especially for relatively high viscosity shear thinning materials. The mechanism by which air entrains in the domain has been studied numerically and experimentally [7, 13, 14] and it has been found that at a fixed flow rate when the substrate speed is high, the dynamic contact line will be instable and eventually the contact line becomes jagged and patterns in the shape of a saw-teeth appear. By further increase of the substrate speed air bubbles are formed by one of two mechanisms described by Bhamidipati et al. [15]. The shapes of upstream and downstream meniscus are linked to the type of defects observed in the film. It has been reported that when the upstream meniscus is not pinned at the corner but located on the die's wall, ribbing will occur due to the formation of some vortices [2, 16-18]. By changing the web speed the shape of the upstream meniscus will changed thus the angle made between the meniscus and web will change too. This angle is called the apparent dynamic contact angle ($\theta_{ad}$). It has been found that $\theta_{ad}$ increases by increasing the web speed (or the Capillary number) and at the air entrainment threshold it reaches to its maximum value [8, 12, 18]. The objective of the current study is to find a correlation between the shape of the upstream meniscus and the onset of the air entrainment both numerically and experimentally. To this end a slot die casting apparatus equipped with a visualization system has been designed and built in-house. The transient coating procedure has been simulated using Volume of Fluid (VOF) model embedded in ANSYS/FLUENT software. It has been observed through experimentation that apparent dynamic contact angle increases with the formation of the sawteeth, at which point, the air entrainment speed reaches its threshold or maximum value. The change of the apparent contact angle versus the capillary number and the maximum casting speed have been computed via the numerical simulations, and the results are found to be in good agreement with the conducted experiments.

## 2. Experimental procedure

A roll-feed imaging system (RFIS) is used to cast thin films, monitor the casting procedure, upstream meniscus and also dynamic contact line behavior. The front and side views of the RFIS are shown schematically in Figure 1 (a) and (b). The casting solution is forced by the pressurized Nitrogen to flow through the slot die and onto the moving substrate (here polyterephthalate (PET)). To monitor the dynamic contact line a transparent plate is installed below the slot die and the transparent PET substrate is allowed to move on top of it, as images are simultaneously recorded. To capture the boundary points, at a fixed flow rate the substrate speed is increased gradually and the speed corresponding to the dripping value is found by monitoring the upstream meniscus. The speed corresponding to air entrainment is marked by observation of air bubbles pinching off from the dynamic contact line and their entrainment in the solution.

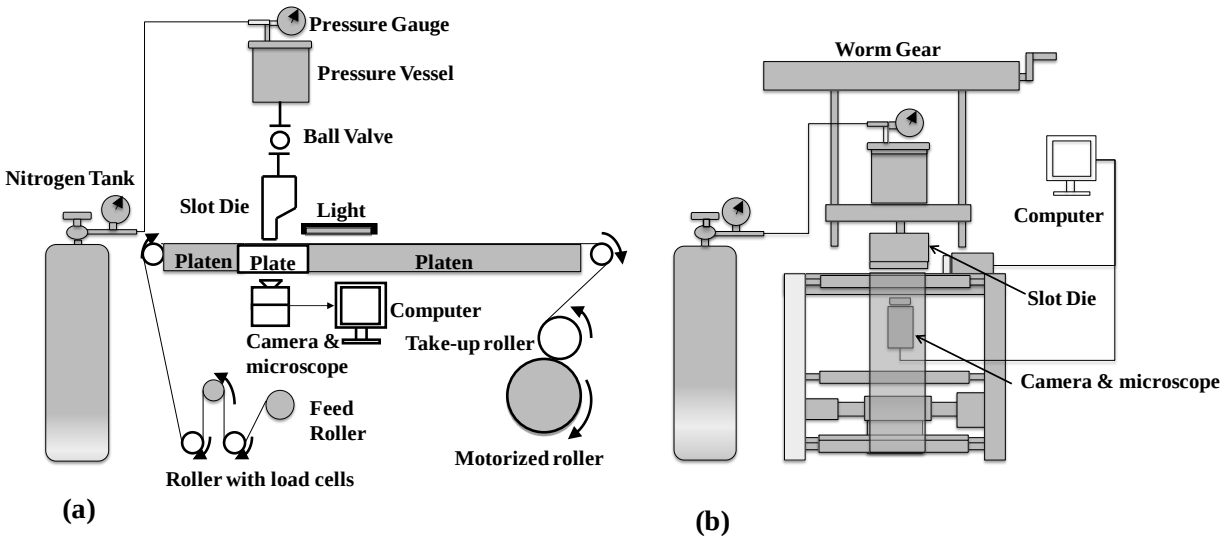


**Figure 1.** Schematic of the experimental set up (a) front view (b) side view.

## 3. Material properties

In this study blackstrap molasses (BSM) a shear-thinning, non-Newtonian fluid with relatively high viscosity is used as the test solution. The viscosity measurement is accomplished using an ARES rheometer. The consistency (k) and the power-law (n) indices are presented in Table 1. The material properties of BSM required for the VOF model are surface tension and the static contact angle ($\theta_s$) of BSM with respect to the PET and stainless steel, which are also listed in Table 1. The surface tension measurement is done by the pendant method and the contact angles on the PET and stainless are measured by Sessile drop method using Ramé-hart Goniometer Model 250.

**Table 1.** Material properties of the test solution.

| **Parameter** | **BSM** |
|---|---|
| Contact angle on stainless steel ($^o$) | 69 |
| Contact angle on PET ($^o$) | 62 |
| Surface tension, $\sigma$ (N/m) | 0.047 |
| Density, $\rho$ (kg/m$^3$) | 1452 |
| Power-law index, n | 0.83 |
| Consistency index, $k$ (Pa-s$^n$) | 8.07 |

## 4. Numerical simulation

The schematic of the numerical domain, its size and also the applied boundary conditions are illustrated in Figure 2. In the casting procedure the pressurized cast solution with a known flow rate ($Q_{in}$) is suspended on the top of the PET, which is moving with the known speed ($u_w$). The cast solution is replacing air, which already exists in the domain. Thus, to simulate the process the transient 2D two phase incompressible and isothermal form of mass and momentum conservation equations are chosen and solved by ANSYS/FLUENT 14 [6-8, 19].

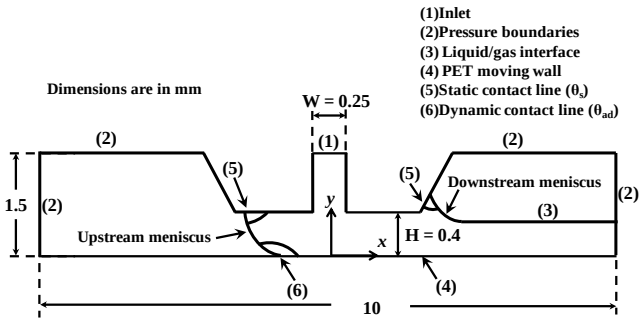


**Figure 2.** Schematic of the numerical domain.

## 5. Result and discussion

For the flow rate of 5 mm/s per unit of width, H = 400 μm and W = 250 μm at different substrate speed the casting process is carried out and the location and the shape of the dynamic contact line and the upstream meniscus are monitored. As shown in Figure 3 at the threshold of air entrainment, saw-teeth are formed and eventually a bubble breaks from their tip. At each substrate speed the dynamic contact angle has been calculated from the extracted pictures, as shown in Figure 3(a). The numerical simulations are carried out for the same set of operating conditions. The numerically calculated values of $\theta_{ad}$ are plotted in Figure 4, against the experimental results. As shown the dynamic contact angle gradually increases from the dripping to the air entrainment threshold.

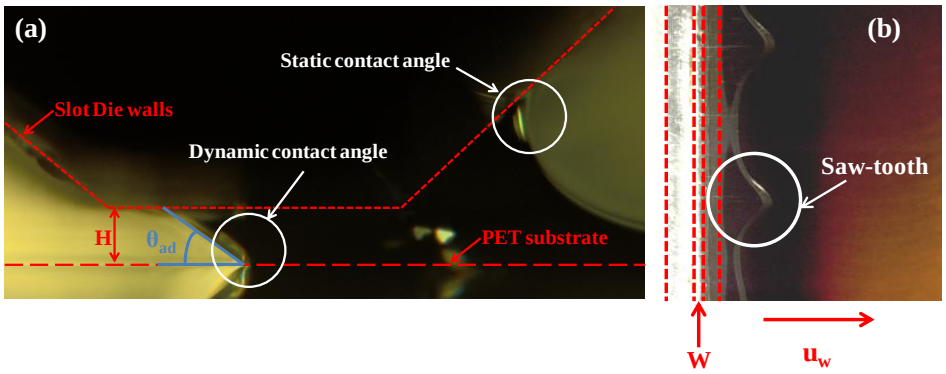


**Figure 3**. (a) Front view, the upstream meniscus (b) The saw-teeth formation at dynamic contact line bottom view.

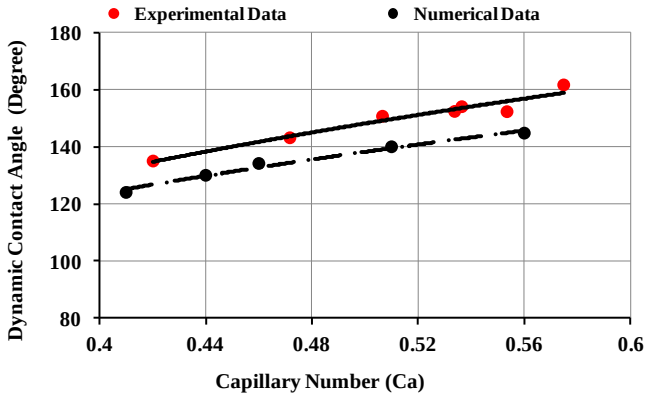


**Figure 4.** Dynamic contact angle versus the capillary number.

## 6. Conclusion

In the current study the change of dynamic contact angle at the upstream meniscus versus the capillary number has been computed numerically and the results are verified by the experimentally obtained data. The relatively small deviation between the numerical and experimental data (less than 11%) can be due to the existence of noise in the system, which can cause more instability, thus higher dynamic contact angle. It has been found that at the point of air entrainment the contact line will become unstable and saw-teeth will appear, at which point air bubbles will pinch off. It has been also found that the dynamic contact angle will increase with increasing Capillary number and at the threshold of air entrainment will reach to its maximum value, approximately160°.

## 7. References


[1] A. E. Beguin, 1954.
[2] E. B. Gutoff and C. E. Kendrick, AIChE Journal 33 (1987) 141.
[3] C.-Y. Ning, C.-C. Tsai, and T.-J. Liu, Chemical Engineering Science 51 (1996) 3289.
[4] C. K. Yang, D. S. H. Wong, and T. J. Liu, Polymer Engineering & Science 44 (2004) 1970.
[5] K. J. Ruschak, Chemical Engineering Science 31 (1976) 1057.
[6] W.-B. Chu, J.-W. Yang, Y.-C. Wang, T.-J. Liu, C. Tiu, and J. Guo, Journal of Colloid and Interface Science 297 (2006) 215.
[7] K. L. Bhamidipati, S. Didari, P. Bedell, and T. A. L. Harris, Journal of Non-Newtonian Fluid Mechanics 166 (2011) 723.
[8] Y.-R. Chang, C.-F. Lin, and T.-J. Liu, Polymer Engineering & Science 49 (2009) 1158.
[9] Y.-R. Chang, H.-M. Chang, C.-F. Lin, T.-J. Liu, and P.-Y. Wu, Journal of Colloid and Interface Science 308 (2007) 222.
[10] B. G. Higgins and L. E. Scriven, Chemical Engineering Science 35 (1980) 673.
[11] M. S. Carvalho and H. S. Kheshgi, AIChE Journal 46 (2000) 1907.
[12] O. J. Romero, L. E. Scriven, and M. S. Carvalho, Journal of Non-Newtonian Fluid Mechanics 138 (2006) 63.
[13] T. A. L. Harris and K. L. Bhamidipati, ECS Transactions 12 (2008) 251.
[14] K. L. Bhamidipati and T. A. L. Harris, ASME Conference Proceedings 2009 (2009) 695.
[15] S. D. K. L. Bhamidipati, and T. A. L. Harris, Chemical Engineering Science Accepted (2012)
[16] C.-F. Lin, B.-K. Wang, C. Tiu, and T.-J. Liu, Advances in Polymer Technology (2012) n/a.
[17] K.-Y. Lee, L.-D. Liu, and L. Ta-Jo, Chemical Engineering Science 47 (1992) 1703.
[18] C.-F. Lin, D. S. H. Wong, T.-J. Liu, and P.-Y. Wu, Advances in Polymer Technology 29 (2010) 31.
[19] ANSYS, 2012.